Z. Kristallogr. **2012**, *227*, 777–792 / **DOI** 10.1524/zkri.2012.1567

Calcite distribution and orientation in the tergite exocuticle of the isopods *Porcellio scaber* and *Armadillidium vulgare* (Oniscidea, Crustacea) – a combined FE-SEM, polarized SCμ-RSI and EBSD study

Bastian H. M. Seidl[I], Christian Reisecker[II], Sabine Hild[II], Erika Griesshaber*[,III] and Andreas Ziegler[I]

[I] Central Facility for Electron Microscopy, University of Ulm, Albert-Einstein-Allee 11, 89069 Ulm, Germany
[II] Institute of Polymer Science, Johannes Kepler Universität Linz, Altenbergerstraße 69, 4040 Linz, Austria
[III] Department of Earth and Environmental Sciences, LMU, Theresienstr. 41, 80333 München, Germany

Received July 28, 2011; accepted September 5, 2012
Published online: October 22, 2012

ACC / Calcite / Orientation patterns of calcite in terrestrial isopods / Isopoda / Texture and function / Mesocrystallinity / Confocal Raman microscopy / EBSD

Abstract. The crustacean cuticle is a bio-composite consisting of hierarchically organized chitin-protein fibres, reinforced with calcite, amorphous calcium carbonate and phosphates. Comparative studies revealed that the structure and composition of tergite cuticle of terrestrial isopods is adapted to the habitat of the animals, and to their behavioural patterns to avoid predation. In this contribution we use FE-SEM, polarized SCμ-RSI and EBSD to investigate micro- and nano-patterns of mineral phase distribution and crystal orientation within the tergite cuticle of the two terrestrial isopod species *Armadillidium vulgare* and *Porcellio scaber*. The results show that the proximal regions of the exocuticle contain both calcite and ACC, with ACC located within the pore canals. Calcite forms hierarchically organised mesocrystalline aggregates of similar crystallographic orientation. Surprisingly, *c*-axis orientation preference is horizontal in regard to the local cuticle surface for both species, in contrast to mollusc and brachiopod shell structures in which the *c*-axis is always perpendicular to the shell surface. The overall sharpness of calcite crystal orientation is weak compared to that of mollusc shells. However, there are considerable differences in texture sharpness between the two isopod species. In the thick cuticle of the slow-walking *A. vulgare* calcite is more randomly oriented resulting in more isotropic mechanical properties of the cuticle. In contrast, the rather thin and more flexible cuticle of the fast- running *P. scaber* texture sharpness is stronger with a preference of *c*-axis orientation being parallel to the bilateral symmetry-plane of the animal, leading to more anisotropic mechanical properties of the cuticle. These differences may represent adaptations to different external and/or internal mechanical loads the cuticle has to resist during predatory attempts.

* Correspondence author
(e-mail: E. Griesshaber@lrz.uni-muenchen.de)

1. Introduction

Arthropods have a cuticle that surrounds the animal completely. It serves as an exoskeleton for support of organs and muscle contractions, as well as an integument providing sensory organs and general protection against environmental strains including predation. Three distinct layers, the exocuticle, the endocuticle, and the membranous layer are composed of chitin-protein fibrils arranged in a twisted plywood structure (Bouligand, 1972). A rather thin fourth layer, the epicuticle, contains waxes and proteins but no chitin. It plays an important role in the formation of surface structures and, in terrestrial species, as a barrier for evaporative water-loss. The mechanical properties of the cuticle can vary considerably, depending on the function of specific skeletal elements in different regions of the animal's body. Factors that influence the mechanical properties of the cuticle include the protein types, the protein-chitin ratio, volume fraction of organic materials and pore canals, water content, the degree of cuticle sclerotisation and the structural organisation of the cuticle (Nikolov *et al.*, 2011; Nikolov *et al.*, 2010; Vincent & Wegst, 2004).

In Crustacea the exo- and endocuticle are reinforced by a mineral phase that can consist of varying amounts of calcite, amorphous calcium carbonate (ACC) and amorphous calcium phosphate (ACP) (Becker *et al.*, 2005; Boßelmann *et al.*, 2007; Neues *et al.*, 2007). The relative amounts and distribution of these minerals are particularly well studied in Isopoda (Becker *et al.*, 2005; Hild *et al.*, 2008; Hild *et al.*, 2009; Neues *et al.*, 2011; Neues *et al.*, 2007; Seidl *et al.*, 2011). It appears that the relative amounts and the distribution of mineral phases depend on the specific function of a skeletal element, and on the habitat and the behaviour of the animal.

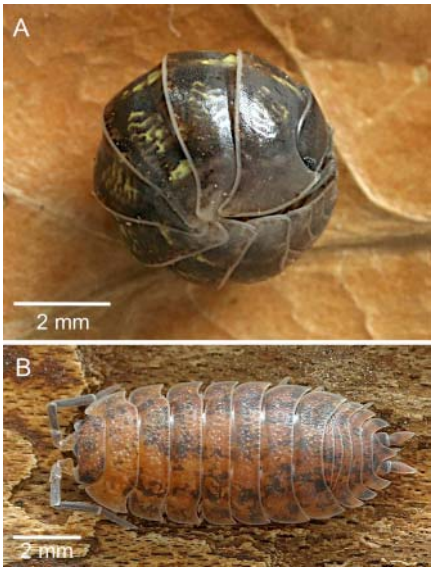

Fig. 1. Images of terrestrial isopods:
(**A**) *A. vulgare* (Latreille, 1804);
(**B**) *P. scaber* Latreille, 1804.

Terrestrial isopods can be grouped into several morphological types that have different ecological strategies and behavioural patterns (Schmalfuss, 1984). Three of these eco-morphological types, the rollers, the clingers and the runners, differ in their behaviour to avoid predation. Even though the body size of *A. vulgare* and *P. scaber* is comparable, the general cuticle thickness is distinct and appears to be linked to the different defensive strategies. *A. vulgare* is a typical roller (Fig. 1A). It walks slowly, has short legs, and the dorsal parts of the thoracic and abdominal body segments (tergites) have an arced cross-section to allow for conglobation. To avoid predation the animal rolls into a sphere (Fig. 1A), relying on the thick and strong cuticle of the tergites to protect its softer ventral side. In addition, when walking on an oblique substrate, conglobation causes the animal to roll away, often into crevasses that may be inaccessible for predators. In contrast, the tergites of *P. scaber* (Fig. 1B) are less arced and are rather thin and flexible. Upon predation it first stands still for a moment and then clings tightly to the substrate to protect its ventral surface. Furthermore, having long legs, *P. scaber* can move fast, and running away is another option for the animal to avoid predation (Schmalfuss, 1984). Since the animals have about the same body size, the differences in general cuticle thicknesses, as well as the thicker calcite layer in *A. vulgare* in comparison to tergites of *P. scaber*, appear to be linked to the different strategies to avoid predation.

In both species calcite and ACC occur within distinct layers (Hild *et al.*, 2008). The endocuticle contains ACC that is isotropic, whereas the anisotropic calcite is restricted to the exocuticle with little ACC overlap. The texture of calcite within the isopod cuticle, which is an important factor for the mechanical properties of the cuticle, is still unknown. For the beach dwelling terrestrial isopod *Tylos europaeus,* location, size and variations in orientation of calcite crystallites have been demonstrated using polarised scanning confocal μ-Raman spectroscopic imaging (SCμ-RSI) (Seidl *et al.*, 2011). This method allows detecting crystallites of different orientation by imaging the intensity ratio of the Raman band indicating crystal lattice vibrations and that for carbonate symmetric stretching vibrations (Porto *et al.*, 1966). Quantifying orientation between crystallites by polarised SCμ-RSI, however, is challenging because this would require analysing each crystallite from various directions. In recent years electron backscatter diffraction analysis (EBSD) has increasingly been employed to study biological carbonate-based skeletal structures (Schmahl *et al.*, 2004; Griesshaber *et al.*, 2007; Goetz *et al.*, 2011; Schmahl *et al.*, 2012). This method allows to unambiguously determine crystal phase and orientation by using Kikuchi line patterns that form by interference of electrons scattered back from discrete crystal lattices (Schmidt and Olesen 1989).

In an attempt to learn more about the distribution and pattern of calcite crystal orientation within the exocuticle of terrestrial isopods we studied microtome polished and etched surfaces of tergite cuticle of *A. vulgare* and *P. scaber* by field emission scanning electron microscopy (FE-SEM), SCμ-RSI and electron EBSD.

2. Materials and methods

2.1 Sample preparation

Tergites of *A. vulgare* (Latreille, 1804) and *P. scaber* Latreille, 1804 were dissected in 100% Methanol and air-dried. The tergites were glued onto cylindrical aluminium holders with a diameter of 3 mm. Samples were cut with a Leica Ultracut ultra-microtome using first glas knifes to expose a sagital or tangential face of the tergite, that was subsequently polished using a 35° Diatome diamond knife by the method described in Fabritius *et al.* (2005). For preparation of cleaved cuticle samples see Hild *et al.* (2008).

2.2 Field emission scanning electron microscopy of etched samples

Polished samples were etched and chemically fixed by submersion in an etching solution containing 2.5% glutaraldehyde and 0.1 mol L-1 HEPES buffer adjusted to a pH of 8.0 for 20 seconds (Seidl & Ziegler, 2012). At this pH ACC dissolves quickly whereas regions containing calcite remain unaffected. The exposed organic matrix is simultaneously fixed by the glutaraldehyde. The samples were washed 3 times in isopropanol for 10 minutes, critical point dried in a BAL-TEC CPD 030 critical point dryer, rotary shadowed with 4 nm of platinum in a Balzers BAF 300 and analysed with a Hitachi S-5200 FE-SEM at 4 kV using a secondary electron detector.

2.3 Confocal Raman spectroscopy

Raman scattering measurements were carried out on an Alpha 300R Raman microscope developed by WITec (Ulm, Germany), equipped with an NdYag laser (wavelength of 532 nm) for excitation. Spectra were recorded in backscattered geometry using a Nikon objective (50×, NA = 0.80)

and episcopic laser beam illumination at about of 12 mW. The optical resolution in lateral (x- and y-axes) and in vertical (z-axis) direction was about 0.3 µm and 0.5 µm, respectively. Spectral resolution was about 3 cm^{-1} using a diffraction grating with 600 grooves cm^{-1}. A piezo driven feedback-controlled scan stage enables to record spectra with a lateral position accuracy of 4 nm. Rayleigh scattered light was blocked using a holographic edge filter. The incident light (z-direction) was polarized either by 0° ($P_{0°}$) or 90° ($P_{90°}$) in relation to the x-scan axis.

All spectra were recorded with the WitecControl acquisition software (WITec GmbH, Ulm, Germany). Samples were imaged with a raster of 9 pixels per 1 μm^2. At each pixel a full Raman spectrum between 0 and 3750 cm^{-1} was recorded with an integration time of 0.5 s. Employing the WITecProject software (Version 2_08, WITec GmbH, Ulm, Germany) (Schmidt *et al.*, 2005) we integrated for each pixel the values of the band for the external (lattice) vibration between 260–310 cm^{-1} and that of the band for symmetric stretching vibration of carbonate between 1070–1100 cm^{-1} ($\Sigma Carbonate$). For imaging the calcite and total carbonate distributions the respective integrated values were plotted in x–y coordinates after intensity coding in red and orange. A calcite single crystal and amorphous calcium carbonate from sternal deposits of *P. scaber* (Ziegler 1994) were used as references.

2.4 Electron backscatter diffraction

EBSD analyses were performed on polished sample surfaces coated with 6–8 nm of carbon (carbon coater: BALTEC MED 020 coating system). EBSD measurements were carried out with a JEOL JSM 6500 F field emission SEM at an accelerating voltage of 20 kV. The signal from the sample that was tilted to 70° was detected with a Nordlys detector and was indexed by the HKL CHANNEL 5 software. Calcite orientation patterns are given in colour coded EBSD maps and corresponding pole figures. Inverse pole figure colouring has been used in all figures showing EBSD data sets. For both isopod species, we mapped tergites of three different animals.

3. Results

3.1 Distribution of calcite within the exocuticle of tergites

The cuticle of *A. vulgare* is about 40 µm thick and thus 2–3 times as thick as the tergite cuticle of *P. scaber*. In cleaved samples of both species two layers can be distinguished in the exocuticle (Fig. 2 and Hild *et al.*, 2008): a distal exocuticle of smooth appearance and a proximal one of rough appearance. The distal, calcite-containing layer is about 8 µm in *A. vulgare* (Fig. 2A, B), while it is 4 µm thick in *P. scaber* (Fig. 2C, D). For *P. scaber* it has been shown that the pore canals are filled with mineral (Fig. 2E) (Seidl and Ziegler 2012).

ACC dissolves easily even at high pH values at which calcite remains stable. Since the tergites of *A. vulgare* and *P. scaber* consist mainly of crystalline and amorphous calcium carbonate, etching of polished surfaces can be used to allocate the distribution of these mineral phases. The results obtained by FE-SEM show that mineral is etched away at the polished surface of the whole endocuticle. This exposes the organic matrix of the tergites consisting of chitin-protein fibrils, which are organised in the typical twisted plywood arrangement, as well as of vertically oriented fibrils that lie inside of the pore canals (Fig. 3A and C). Within the exocuticle, distal areas that are about 7 µm in *A. vulgare* and 2.5 µm thick in *P. scaber* remain unaffected by the treatment with etching solution, indicating the presence of calcite (Fig. 3A, C). In the remaining proximal areas of the exocuticle most regions appear to contain calcite as well, however, ACC occurs within distinct regions exposing fibres that are mostly oriented vertically and that are not organised in a twisted plywood arrangement. In *A. vulgare* these regions are about 300 nm thick and often interconnect with each other (Fig. 3B). In *P. scaber* these ACC containing regions appear thinner and interconnect less frequently than those in *A. vulgare* (Fig. 3D).

3.2 Raman spectroscopic imaging of crystal orientation

The Raman spectrum for calcite has characteristic lattice vibration bands at 158 and 284 cm^{-1}, carbonate bending vibration at 715 cm^{-1}, and carbonate stretching vibration at 1090 cm^{-1} (Fig. 4a). For biogenic amorphous calcium carbonate the carbonate stretching vibration broadens and shifts to lower values, and a broad band ranging from 100–350 cm^{-1} replaces the bands for calcite lattice vibrations (Fig. 4b). Bands ranging from 2900–3000 cm^{-1} and from 3000 to 3500 cm^{-1} that are typical for organic materials and water, respectively, indicate the biological origin of the ACC sample (Fig. 4b).

Raman spectra acquired by applying polarized laser excitation yields information about the orientation of molecules within the sample towards the incident light (Porto *et al.* 1966; Kondilenko *et al.* 1976; Tyrrell 1984). To estimate the correlation between crystal orientation and the polarization angle of the incident light we recorded Raman spectra of a geological calcite. The cleaved crystal was mounted on the scanning table so that the z-direction of the incident laser light was oriented perpendicular to one of the faces of the {1014} calcite cleavage rhombohedra (Fig. 4c). The crystal was alligned with the projection of the c-axis parallel to the polarisation of the incident light ($P_{0°}$). When the polarization of the incident light is switched by 90° ($P_{90°}$) $\Sigma Carbonate$ intensity increases by a factor of 3 in relation to $\Sigma Calcite$ (Fig. 4a). In contrast, changing polarization has little effect on $\Sigma Carbonate$ intensity in spectra recorded from ACC (Fig. 4b). When the polarizer is stepwise rotated from −90° to 90°, absolute values for the integral intensity of the two bands continuously change in opposing directions with $\Sigma Carbonate$ decreasing by more than twice and $\Sigma Calcite$ increasing by a factor of about 1.5, with a minimum value for $\Sigma Carbonate$ and a maximum of $\Sigma Calcite$ at 0° of the polariser (Fig. 4D). Thus, the intensity ratio

$$CR = \Sigma Calcite / \Sigma Carbonate$$

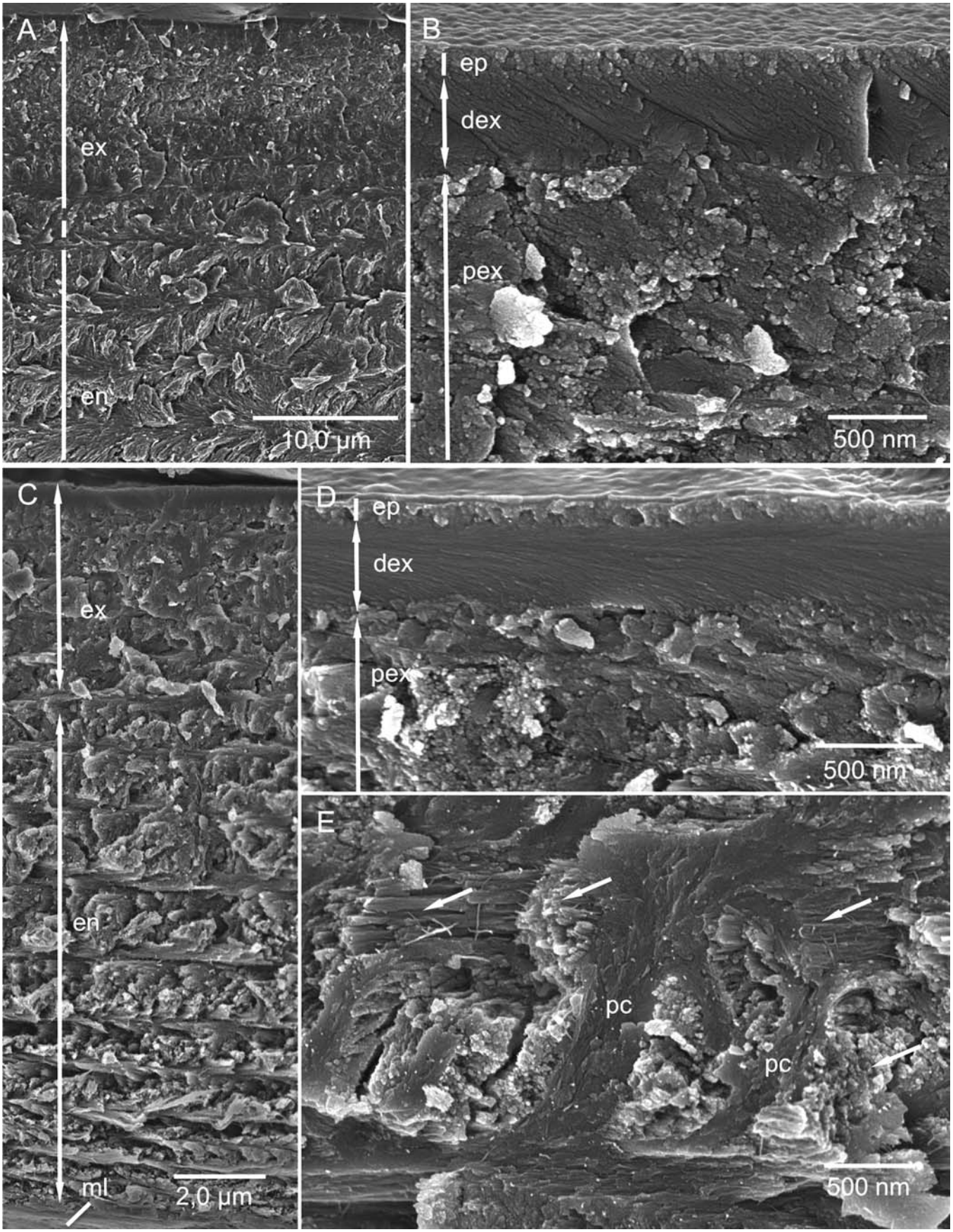

Fig. 2. Field-emission scanning electron micrographs of sagittally cleaved non-decalcified tergites of *A. vulgare* (**A**, **B**) and *P. scaber* (**C–E**). (**A**, **C**) Overview of the exocuticle (ex), endocuticle (en); ml, membraneous layer. (**B**, **D**) Structure of the outer region of the exocuticle. The cleaved distal exocuticle (dex) has smooth appearance in comparison to the subjacent proximal exocuticle (pex); ep, epicuticle. (**E**) pore canals (pc) filled with mineral within the proximal exocuticle; arrows, mineralized protein-chitin fibres arranged according to the twisted plywood structure.

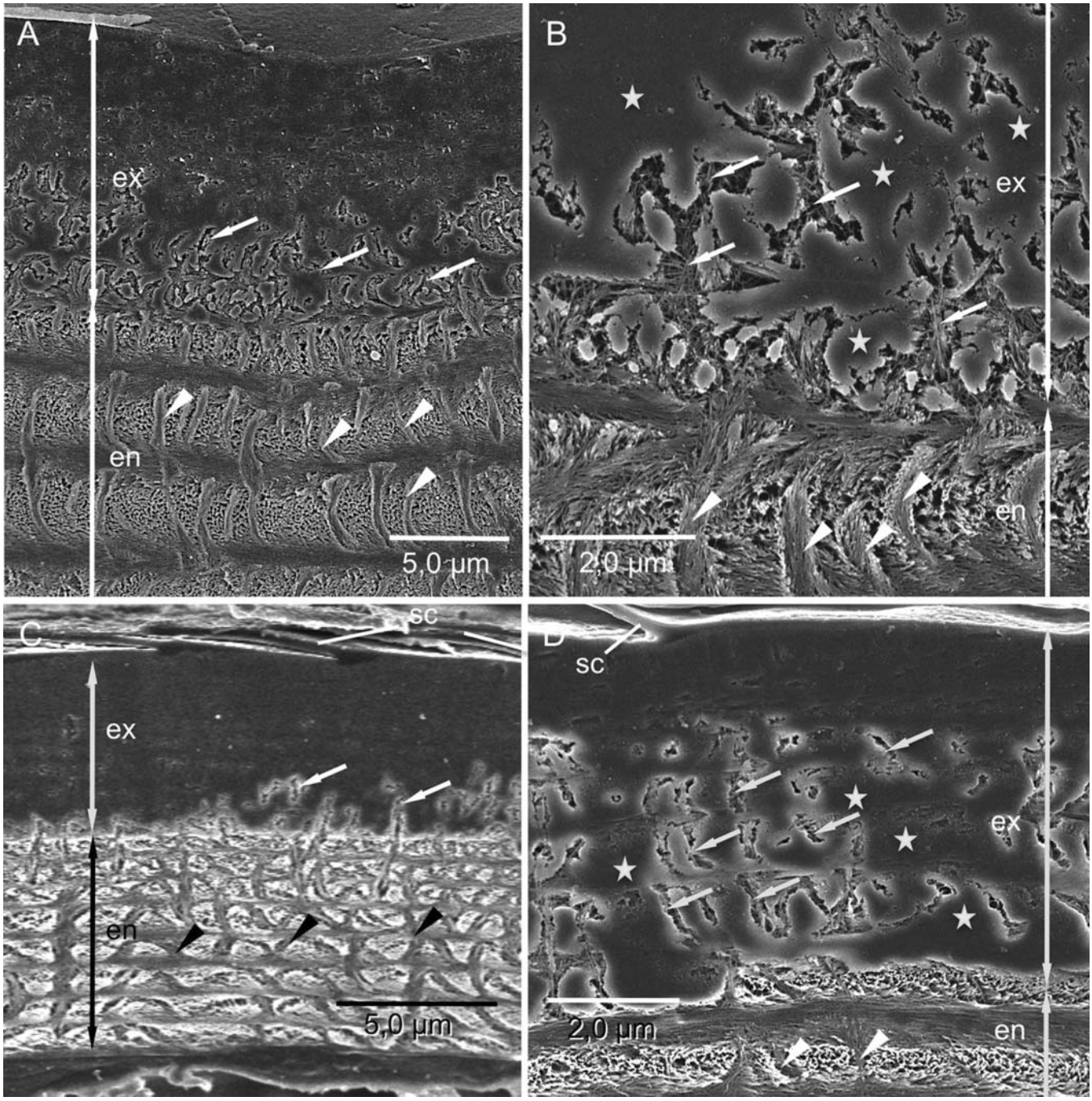

Fig. 3. Field-emission scanning electron micrographs of sagittally polished and etched surfaces of non-decalcified tergites of *A. vulgare* (**A**, **B**) and *P. scaber* (**C**, **D**). (**A**, **C**) Overview of exocuticle (ex) and endocuticle (en). The surface in the endocuticle is completely etched indicating that it contains amorphous calcium carbonate but no calcite; arrowheads: pore canals within the endocuticle; arrows: etched regions within the exocuticle. Most regions of the exocuticle remain unaffected and thus indicate the presence of calcite. (**B**, **D**) Details of the regions at the border between endo- and exocuticle. Within the exocuticle unetched regions (asterisks) indicate the presence of calcite.

can be used to estimate the orientation of calcite. For the investigated calcite crystal a 3 fold increase in CR from about 0.4 at 90° to 1.2 at 0° has been found. This shows that for a calcite crystallite with a given x–y-component of the crystallographic c-axis, switching the polarizer by 90° would results in changes of CR by a factor between 2.5 and 3 when the c-component would be oriented parallel or perpendicular to the initial polarization of the incident light. The ratio of CR varies only by factor 1 to 2 for configurations in between these orientations (Fig. 4e).

Raman maps of sagittal planes of *A. vulgar*e (Fig. 5a, b) and *P. scaber* (Fig. 6a, b) cuticle recorded for 0° and 90° polarized incident light show that the crystalline layer is confined within the outer 10–15 µm and 3–5 µm of the cuticle, respectively. These regions correspond well in location and thickness to the exocuticles of the two species. The carbonate signal below the exocuticle results from amorphous calcium carbonate (ACC) within the endocuticle. Furthermore, the maps for both sagittal and tangential planes reveal calcite crystallites with distinct domains of crystallographic orientation for both species. This aspect becomes particularly well visible when mapping the normalized intensity CR, since measurements of cleaved calcite showed that reliable conclusions on crys-

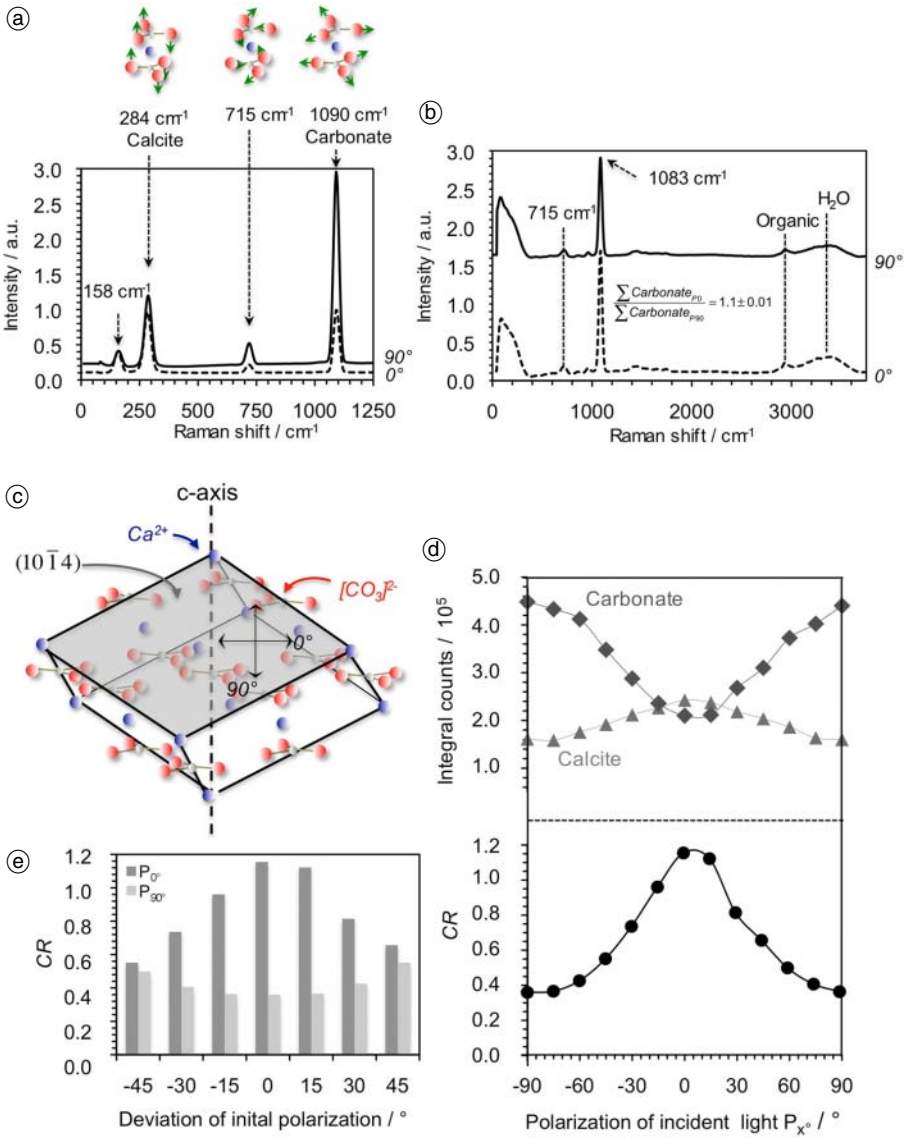

Fig. 4. Effect of polarization of the incident light on Raman spectra of calcium carbonate. All spectra were recorded with the incident laser light perpendicular to the sample faces. (**a**) Raman spectra for calcite using polarizations of 0° and 90°, depicting changes in relative intensity for external (lattice), and internal carbonate stretching vibrations. (**b**) Effect of polarization on biogenic amorphous calcium carbonate (ACC). (**c**) Schematic drawing of a calcite cleavage rhombohedra displaying the spatial arrangement of the Ca^{2+} and CO_3^{2-} ions, the crystallographic *c*-axis and the Miller-Bravais index associated with one of the faces. (**d**) The integral intensity of lattice vibration (Σ*Calcite*) and that of the carbonate stretching vibration (Σ*Carbonate*) in dependence of the polarization of the incident light. The intensities follow continuous curves with opposed progressions (upper graphs). (**e**) CR changes for deviation of polarizer between −45° and +45° for calcite *c*-axis orientation perpendicular P_0 and parallel P_{90} to the initial polarization of the incident light. Note that the largest deviations occur in the perpendicular configuration.

tallographic orientation can be deduced from CR values only.

In sagittal planes of *A. vulgare* three regions can be distinguished within the crystalline layer of the exocuticle: a thin layer close to the surface with 1–2 µm thickness, followed by a 6–8 µm thick region with well-defined domains of different CR values in the middle, and a proximal 2–3 µm thick layer within which CR hardly changes with variation in polarization. The constant CR value within the proximal layer is probably due to the overlap with the endocuticle that contains ACC rather than calcite and thus is no indication for a high texture.

The values of CR in sagittal planes vary between 0.1 and 0.5. Raman images of tangential planes through the exocuticle of *A. vulgar*e and the corresponding CR maps show well the lateral extension of crystallites with similar crystallographic orientation (Fig. 5c, d). In tangential planes the maximum values for CR are in the range of 0.8. Comparing individual areas within the CR maps obtained for 0° and 90°, the corresponding CR can switch from 0.2–0.3 to values larger than 0.6.

In *P. scaber* subregions of calcite with varying crystallographic orientation can well be identified in both sagittal and tangentially polished planes. For this species maximum CR values of about 0.8 in both planes were observed (Fig. 6). Nominally tangential planes through the cuticle of *P. scaber* were actually directed through cuticular tubercles (see SEM image in Fig. 7) resulting in oblique planes through the local cuticle surface and in a large central region containing ACC only (Fig. 6c, d). In some regions of the tergite cuticle of *P. scaber* the calcite layer seems to be subdivided into two layers: a distal layer with varying CR values and a proximal one with lower and less varying CR values (Fig. 6).

3.3 Orientation patterns of calcite within the exocuticle of tergites

SEM images show that the orientation of polished planes deviate only little from the surface of the tergite cuticle of *A. vulgare* (Fig. 7A), whereas in *P. scaber* the polished plane lies within tergite tubercles (Fig. 7B). This results in local variations of the angle between the exposed plane and the cuticle surface that depend on the cutting distance from the tubercle tip (see also discussion within the following paragraph). Inversed pole figure colour coded

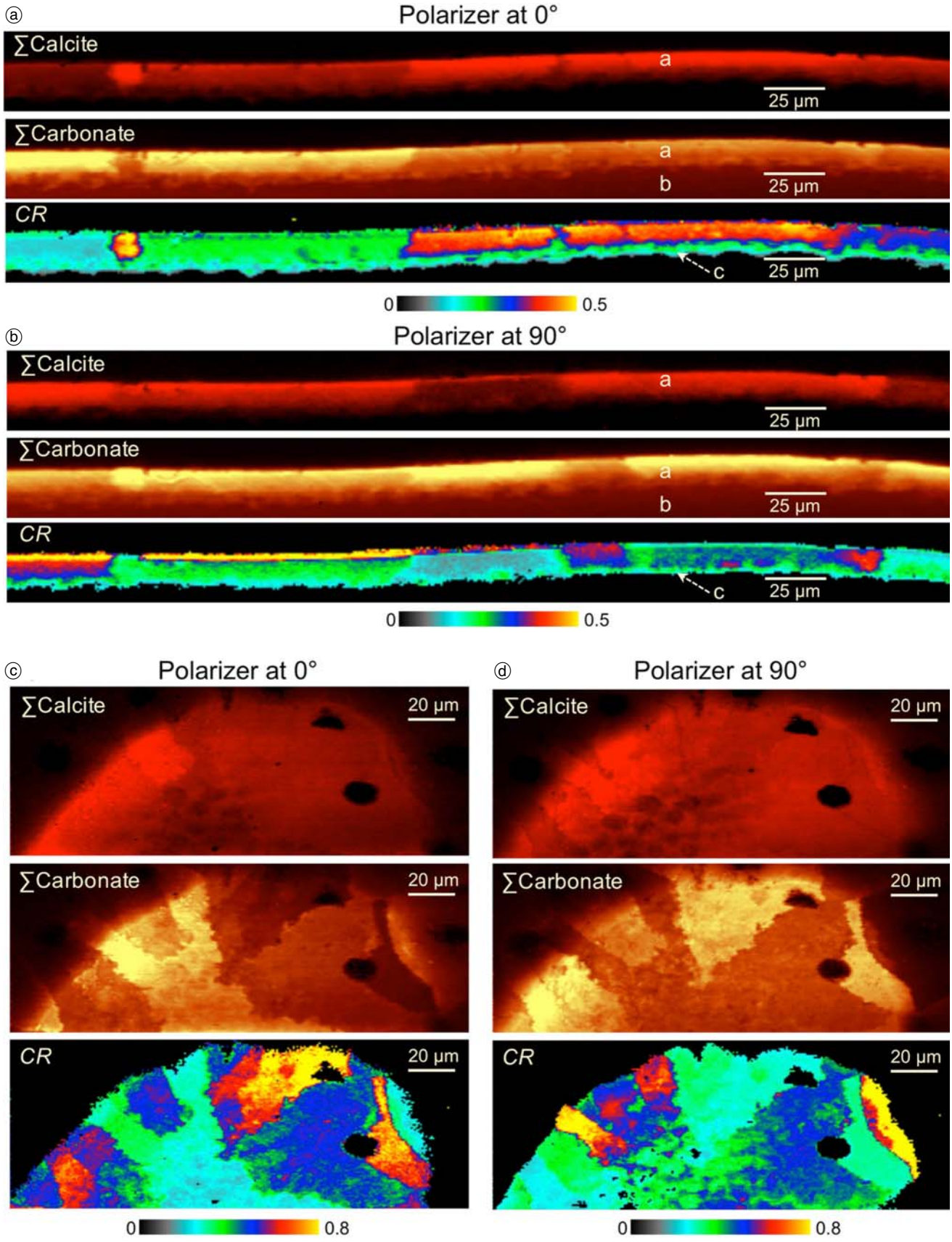

Fig. 5. Raman images showing maps for *ΣCalcite* (red), *ΣCarbonate* (orange) and the calculated ratio CR = (*ΣCarbonate*)/(*ΣCalcite*) recorded for 0° and 90° polarized incident light of sagittal (**a**, **b**) and tangential (**c**, **d**) plains of *A. vulgare* tergite cuticle. The crystalline layer (a) is within the outer 10 µm of the cuticle (*ΣCalcite*) (**a**, **b**). The *ΣCarbonate* signal below this region is due to the presence of ACC (b). Changes in the intensity between 0° and 90° polarization indicate domains containing calcite with different crystallographic orientation (**a–d**). The maps for tangential planes reveal an irregular shape of the calcite domains (**c**, **d**). CR maps of sagittal planes show 3 distinct calcite layers, the proximal 2–3 µm thick transition layer (c) is due to the overlap of calcite and ACC. Note that maximum CR value in tangential planes is higher (0.8) than in sagittal planes (0.5).

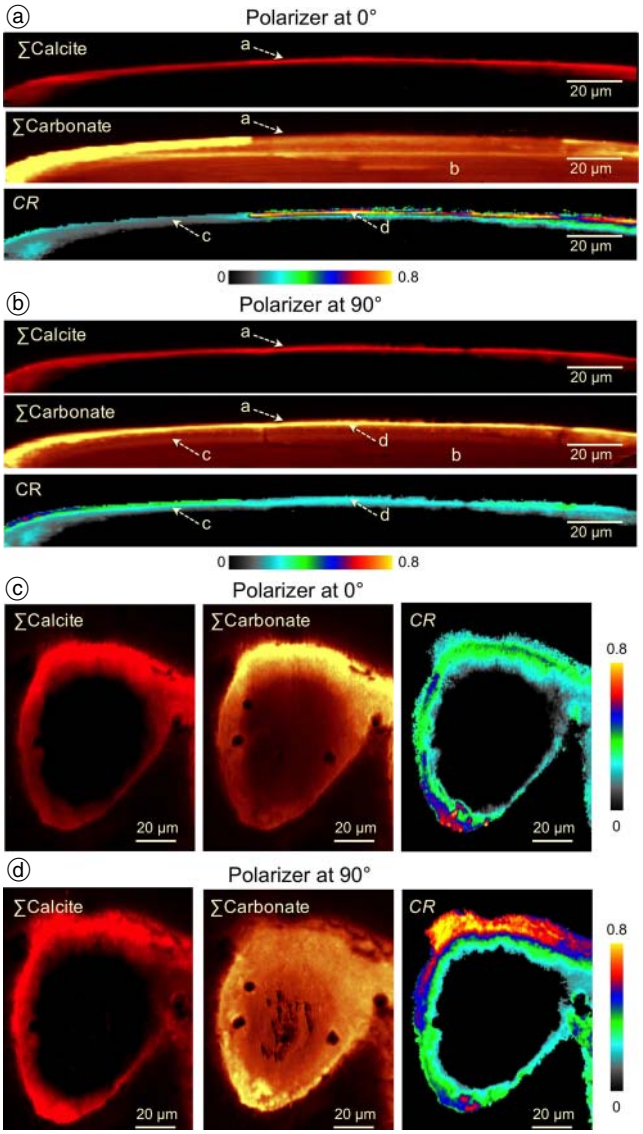

Fig. 6. Raman images showing maps for *ΣCalcite* (red), *ΣCarbonate* (orange) and the calculated ratio CR = (*ΣCarbonate*)/(*ΣCalcite*) recorded for 0° and 90° polarized incident light of sagittal plains (**a**, **b**) and nominally tangential plains of *P. scaber* tergite cuticle (**c**, **d**). The latter plains are parallel to the general surface of the cuticle but were actually directed through cuticular tubercles. The crystalline layer (a) is within the outer 3–5 µm of the cuticle (*ΣCalcite*) (**a**, **b**). The *ΣCarbonate* signal below this region is due to the presence of ACC (b). Changes in the intensity between 0° and 90° polarization indicate domains containing calcite with different crystallographic orientation (**a–d**). Two layers can be discriminated in the region containing calcite: an outer 1–3 µm thick layer, and a 2–3 µm thick transition layer that is due to an overlap between calcite and ACC and does not change CR with variation in polarization (**a–d**).

EBSD maps reveal that the exocuticle of both species contains regions of similar crystallographic orientation (Fig. 7C, D). The corresponding contoured versions of pole figures for *c*- and *a*-axes orientations reveal that these regions result from agglomerations of calcite structures (Fig. 7E, F). The pole figures depict particularly well the high coherence in the crystallographic orientation of calcite within each aggregate, and thus the strength (or sharpness) of the texture. Thus, the tergites of *P. scaber* and *A. vulgare* are composed of individual aggregates with mesocrystalline arrangements of calcite. Within these individual aggregates, calcite has a coherent 3D crystallographic lattice orientation, a coherent orientation of both, the *c*- and *a*-axes. In contrast to the high strength of the texture within aggregates in both species, we find large differences in the all over crystallographic orientation between aggregates (Fig. 7C, D). This becomes particularly clear when we depict pole figures for a number of individual aggregates for *A. vulgare* and *P. scaber* (Fig. 7G, H). EBSD maps and the corresponding pole figures recorded from planes in different depths of the same tergite region show, that, surprisingly, the crystallographic orientation between aggregates is considerably weaker for A. vulgare (Fig. 8A–C) than in the tergite cuticle of *P. scaber* (Fig. 8D–F). This result was confirmed by comparing 102 aggregates from 7 different planes of *A. vulgare* with 21 aggregates from 4 different planes of *P. scaber* cuticle (see Fig. 11 of the Discussion).

The orientation of tangential planes through the cuticle of *A. vulgare* deviates only slightly from the orientation of the cuticle surface (Fig. 7A). However, in *P. scaber* these deviations are high because, as already mentioned above, the planes go through cuticular tubercles (Fig. 7B). Therefore, in *P. scaber*, the orientation of polished planes towards the nearby cuticle surface depends on the distance of the plane from the tip of the tubercle. (Fig. 8D–F). At the most elevated portions of the tubercle the calcite *c*-axes are steep and deviate by about 20 degrees from the plane normal (Fig. 8D, G), and up to 50 and 85 degree in planes through the middle and the base of the tubercle, respectively (Fig. 8E–G). This indicates that calcite *c*-axis in *P. scaber* rotates with the curvature of the cuticle of the tubercles, but also indicates that calcite *c*-axes deviate only by about 5 to 10 degrees from the nearby surface regardless of the position within the tergites. Furthermore, the results show that for *P. scaber* the *c*-axes are oriented more or less along the symmetric (bilateral) anterior-posterior plane of the animal (Fig. 8G).

4. Discussion

Employing a combined analytical approach our study extends previous results on distribution of calcite and amorphous calcium carbonate and provides new results on the crystallographic texture of calcite in two species of terrestrial isopods. We show the presence of both calcite and ACC within proximal regions of the exocuticle, where ACC is mostly located within the pore canals. Investigating the distribution pattern of calcite crystal orientation we reveal that calcite is organized mesocrystalline and in at least four hierarchical levels, and show differences in the all over texture of the tergite cuticle between *A. vulgare* and *P. scaber* that may be of functional significance. Furthermore, we provide the first study where automated EBSD analysis is performed on microtome polished biological hard tissues, and evaluate the use of polarised SCμ-RSI for combined phase and texture analysis.

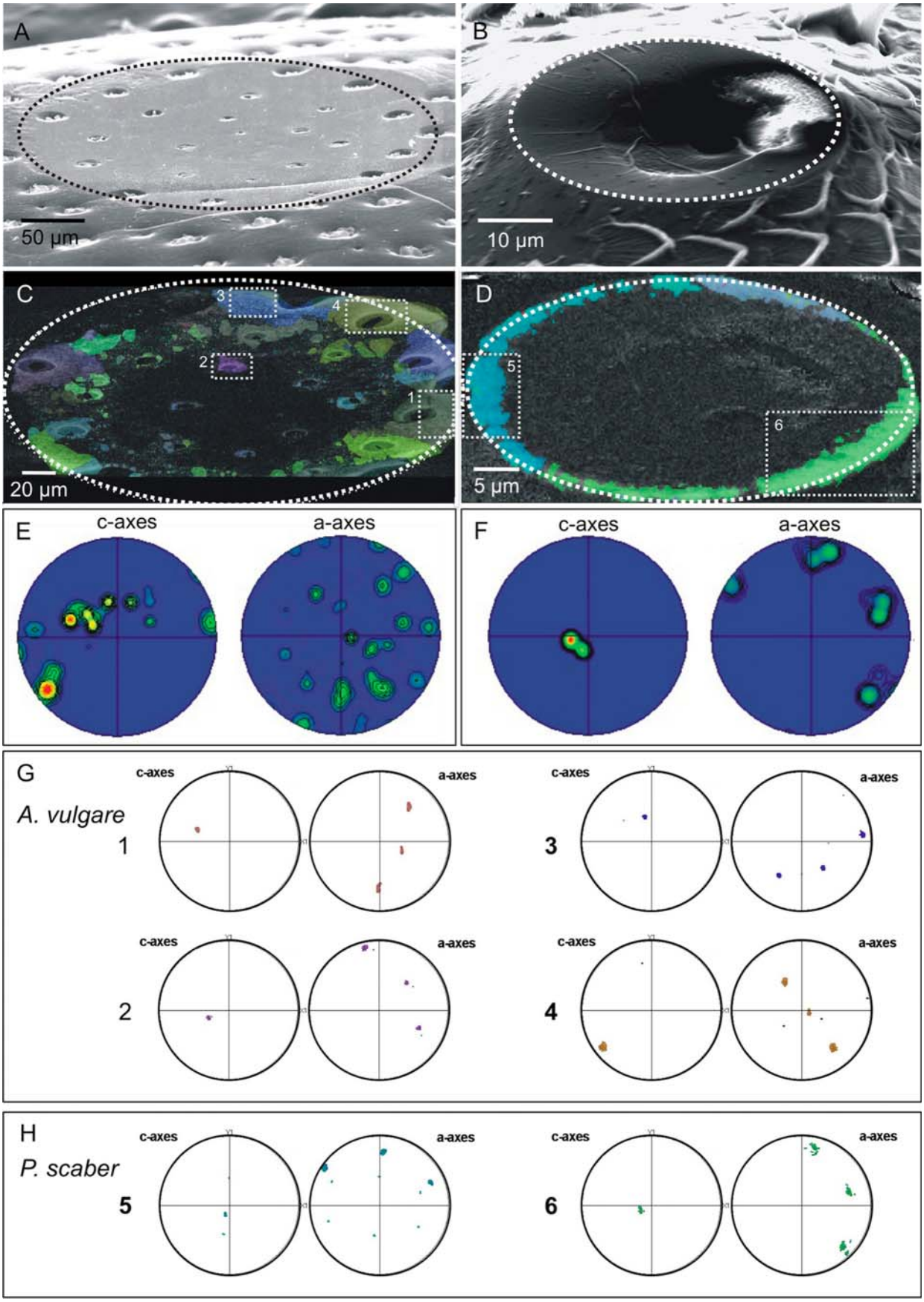

Fig. 7. SEM (**A**, **B**) and EBSD (**C–H**) results obtained from the exocuticle of *A. vulgare* (**A**, **C**, **E**, **G**) and *P. scaber* (**B**, **D**, **F**, **H**). The SEM images give an overview of the tergite regions that were mapped with EBSD. Inverse pole figure color-coded EBSD maps (**C**, **D**), pole-orientation density distributions (**E**, **F**), and pole figures depicting calcite *c*- and *a*-axes orientations (**G**, **H**) of selected regions in (**C**) and (**D**) (numbered rectangles) show the mode and the sharpness of calcite crystal orientation. Within individual calcite aggregates *c*- and *a*-axes orientation coherence is high (**E–H**). In contrast, the overall texture sharpness is low especially in *A. vulgare*, (**E**).

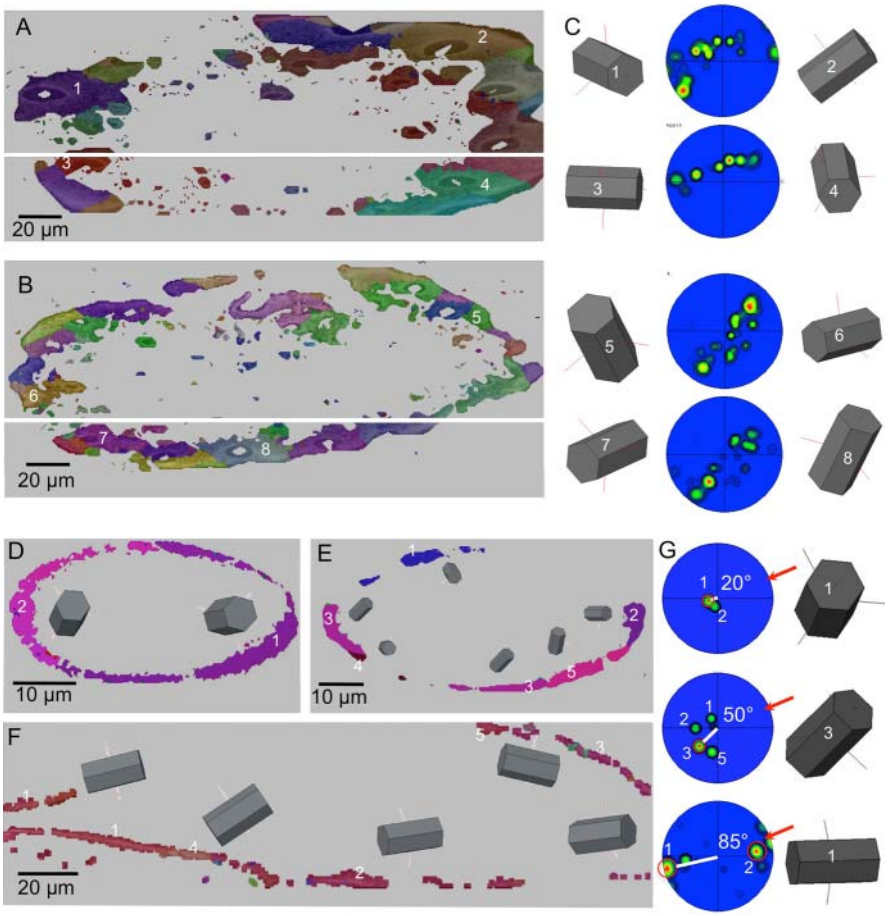

Fig. 8. Variation of *c*-axis inclination in tangential planes of different depths through the smooth cuticle of *A. vulgare* (**A–C**) and a tubercle of *P. scaber* (**D–G**). Inverse pole figure color-coded EBSD maps (**A**: more distal, **B**: more proximal, **D**: more distal **E** and **F**: more proximal). Pole-orientation density distributions (**C**, **G**). In *A. vulgare* calcite occurs in many, more or less randomly oriented aggregates (**C**). In contrast, the calcite aggregates in the cuticle of *P. scaber* contain only a few zones of slightly different orientations (**G**). In the uppermost polished plane through the tubercle calcite *c*-axis is inclined by 20 degrees to the normal of the plane (**A**, **G**). Towards the base of the tubercle this angle of the *c*-axis becomes larger (**E**, **G**) and lies almost parallel to the polished plane at the base (**F**, **G**). Furthermore, the *c*-axes of calcite aggregates appear to be oriented close to the bilateral symmetry plane of the animal (red arrows in **G**).

4.1 Distribution of calcite and amorphous calcium carbonate in tergite cuticle

Our Raman spectroscopic imaging confirms previous results on the general distribution of calcite and ACC within the tergite cuticle of *A. vulgare* and *P. scaber* (Hild *et al.*, 2008). In these species the endocuticle contains exclusively ACC, whereas the main part of the exocuticle is mineralised by calcite. However, because of limits in the spatial resolution of SCμ-RSI, there remained some uncertainty about the distribution of the carbonate phases in the proximal region of the exocuticle for which Raman spectroscopy has indicated the presence of both phases (Hild *et al.*, 2008). The present ultrastructural results on polished and etched planes of tergite cuticle show that this overlap is mostly, if not exclusively, due to mineral filled pore canals that frequently contain ACC in proximal regions of the exocuticle.

Currently we know that the tergite cuticle from 8 terrestrial and 4 marine isopod species contains ACC and Mg-calcite and minor amounts of amorphous calcium phosphate (Becker *et al.*, 2005; Hild *et al.*, 2008; Hild *et al.*, 2009; Neues *et al.*, 2007; Seidl *et al.*, 2011). In four of these species the distribution of calcium-carbonate phases have been studied by SCμ-RSI (Hild *et al.*, 2008; Hild *et al.*, 2009; Seidl *et al.*, 2011). Interestingly, the distribution of carbonate phases and the thickness of the outer calcite layer vary between terrestrial isopod species and is most probably function related. In the up to about 100 μm thick tergite cuticle of the conglobating sand-burrowing beach isopod *T. europaeus* the distal layer of calcite can cover more than one fourth of the cuticle thickness. In contrast, in the cave dwelling isopod *Titanetes albus,* that has a thin cuticle (10 μm) for a rather large animal (20 mm), calcite covers only one tenth of the cuticle thickness and is restricted to the distal part of the exo-

Table 1. Therefore, values provided in the table should be regarded as guide numbers.

Isopod species	Eco-morphological type	Thickness of cuticula* (μm)	Thickness calcite layer within the cuticula* (μm)	Texture
Porcellio scaber	clinger – runner lives on land	20	up to 6	medium, 3D
Armadillidium vulgare	roller lives on land	40	up to 20	low, cylindrical
Tylos europeus	roller lives in burrows in the sand at beaches	up to 100	up to 30	very low, cylindrical

*Note that the thickness of the cuticle also depends on the size of the animal.

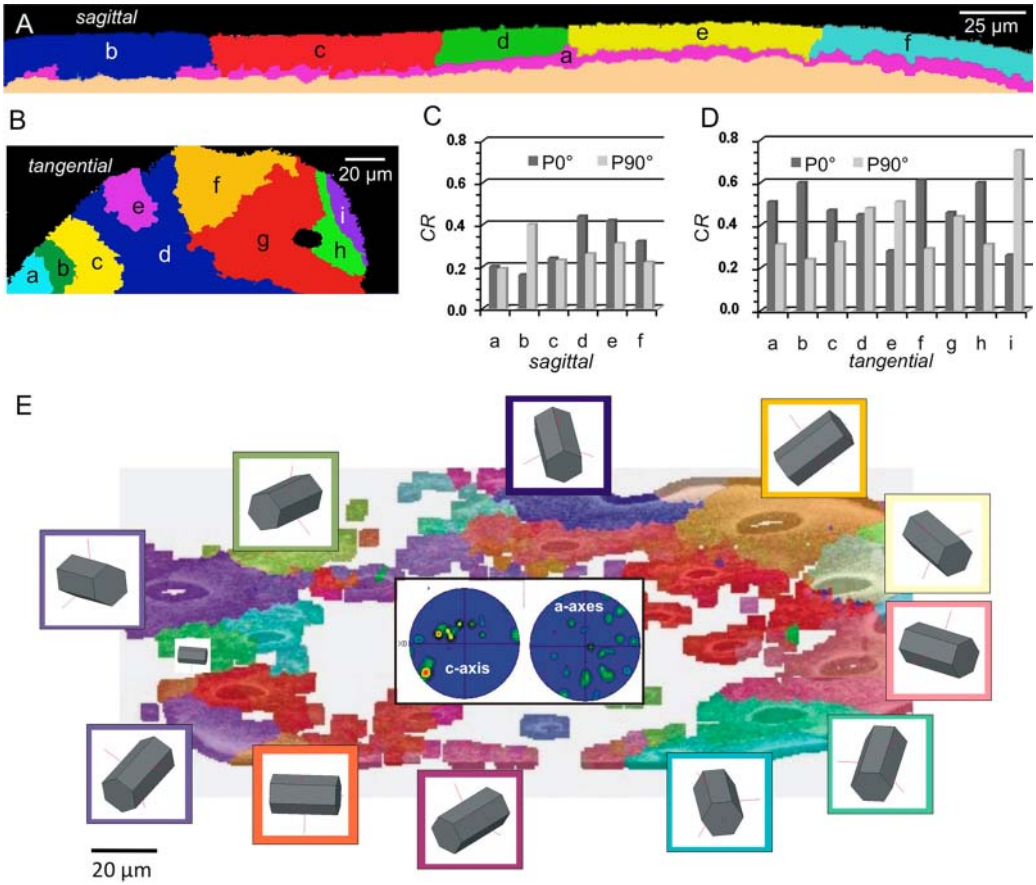

Fig. 9. Comparison of results for calcite axes orientations for *A. vulgare* derived from Raman (**A–D**) and EBSD (**E**) measurements. Areas of similar values of CR = (Σ*Carbonate*)/(Σ*Calcite*) are combined and plotted in the same color for sagittal (**A**) and tangential planes (**B**). The small change in the region (a) in the sagittal plane is probably due to the overlap with the ACC containing region. The individual CR values change between factors of about 1 (c in **C**) and more than 2 (b in **C**) for the sagittal plane, and between 1 (d, g in **D**) and almost 3 (b, I in **D**) for the tangential plane. The high variations in the CR changes for both, sagittal and tangential planes, suggests a preference in the orientation of the *c*-axis of the calcite aggregates parallel to the surface of the cuticle and some variation in the *x*–*y* direction, in agreement with calcite-axes orientation variations deduced from EBSD measurements (**E**).

cuticle. In *T. europaeus* there is a sharp border between the layer containing calcite corresponding to the distal exocuticle and the one containing ACC corresponding to the proximal exocuticle and the endocuticle (Seidl *et al.*, 2011), whereas in *T. albus,* calcite is restricted to roughly the distal half of the exocuticle that contains ACC as well, and ACC occurs in the remaining proximal region of the exocuticle and in the endocuticle (Hild *et al.*, 2009).

It appears that the distribution of calcite within the distal and ACC within proximal layers is of mechanical significance. EDX maps indicate that the difference in the mineral content between exocuticle and endocuticle is negligible in *P. scaber* and only 15% higher in the exocuticle of *A. vulgare* (Hild *et al.*, 2008). Therefore, it appears that differences in the mineral phase between exo and endocuticle is of higher significance than mineral content. Generally the incorporation of $CaCO_3$ into the organic matrix of the cuticle has a great effect on the stiffness of the cuticle (Nikolov *et al.*, 2010). It has been demonstrated that cuticle containing calcite is harder and has a higher Youngs modulus in comparison to that containing ACC (Fabritius *et al.*, 2012). Therefore, the location of calcite towards external loads makes sense. Within a composite material like the crustacean cuticle the poor fracture strength of calcite is strongly attenuated due to the abundant protein-chitin fibres of the organic matrix. The endocuticle that is mineralised with ACC contains such an organic matrix as well, and should thus be less brittle in comparison of the exocuticle. It has been emphasized that a combination of a harder/stiffer distal and a softer/more compliable proximal layer would be beneficial to the animal when the cuticle would be bend in a way that the harder albeit brittle exocuticle would be in compression and the more compliable endocuticle in tension, as it would be the case for external loads onto the cuticle surface (Vincent, 1998).

In terrestrial isopods that rely more on the mechanical strength of their cuticle (rollers) both the calcite containing layer and the subjacent ACC containing layer are thicker than in species that run away to avoid predation (runner) (Table 1). However, here it is of interest that the relative thickness of the calcite-containing layer is lower in the rollers in comparison to that of the runners, resulting in a higher ACC/calcite ratio. A quantitative approach of mineral composition indicates 60%-wt and 38%-wt ACC, and 12%-wt and 16%-wt calcite in the tergite cuticle of *A. vulgare* and *P. scaber,* respectively (Becker *et al.*, 2005). One reason for the difference in the ACC/calcite ratio may be due to the way most terrestrial isopods store calcium carbonate, which probably evolved during the transition from marine to terrestrial habitats, to compen-

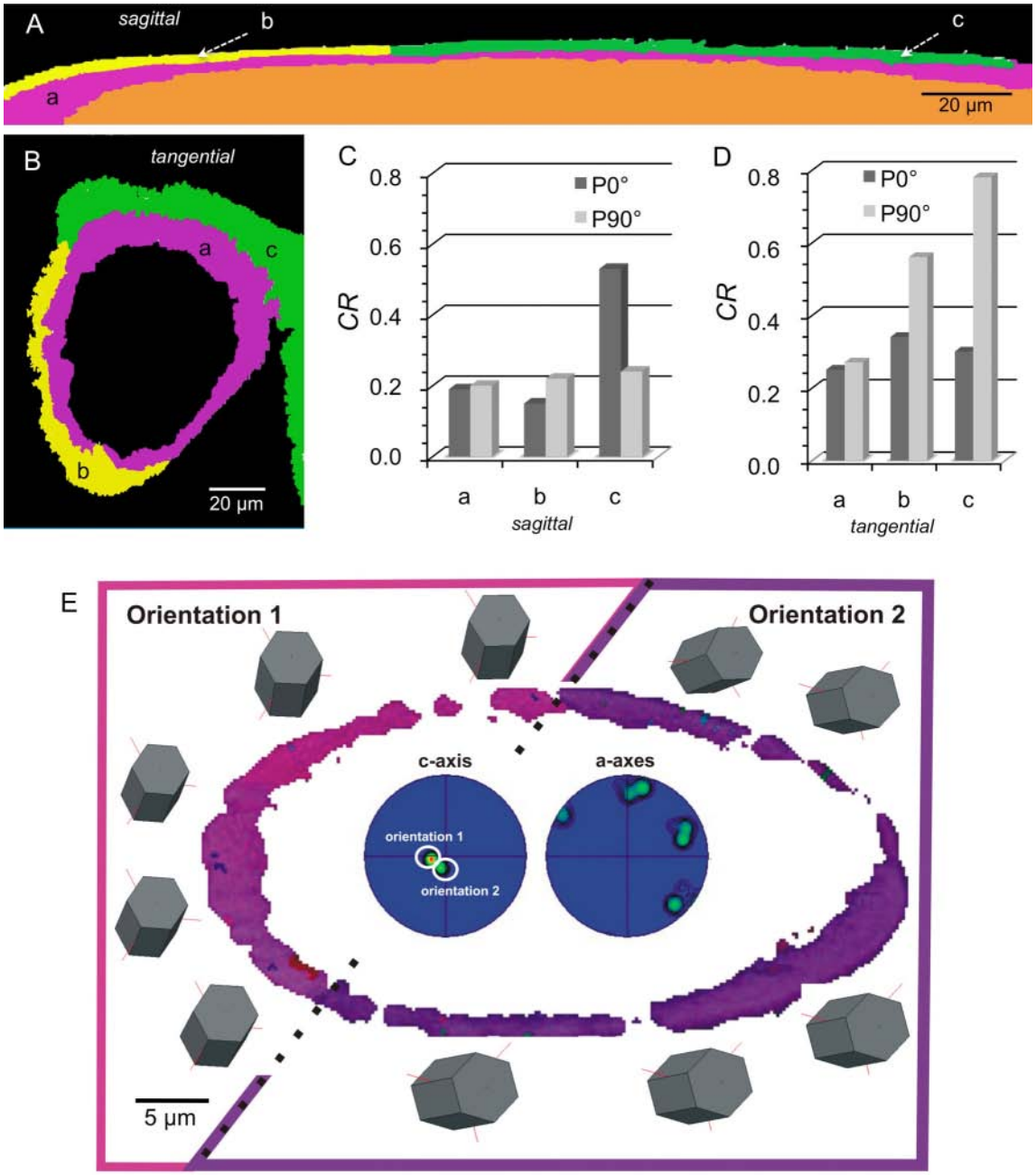

Fig. 10. Comparison of results for calcite axes orientations for *P. scaber* derived from Raman (**A–D**) and EBSD (**E**) measurements. Areas of similar values of CR = (Σ*Carbonate*)/(Σ*Calcite*) are combined and plotted in the same color for a sagittal (**A**) and a tangential plane at the base of a cuticle tubercle (**B**). The small change in the region (a) in both planes is probably due to the overlap with the ACC containing region. The CR values for calcite change by factors of about 1.3 (b in **C**) and 2 (c in **C**) for the sagittal plane and by 1.6 (b in **D**) and 2.6 (c in **D**) for the tangential plane, respectively. Although for *P. scaber* the number of regions analyzed by Raman microscopy is too low to obtain representative data, the lower range of CR changes in comparison to that of *A. vulgare* (Fig. 9) is in accordance to the results obtained by EBSD (**E**) and suggest that in contrast to the cuticle of *A. vulgare* calcite crystals are grouped into few zones with similar orientations.

sate for the slow uptake of calcium ions in a terrestrial environment. Like all Crustacea, in a process called moulting, isopods regularly shed the old cuticle and produce a larger one in order to grow. During the moulting cycle terrestrial isopods resorb ACC from the cuticle and store and recycle it to mineralise the new cuticle (Neues *et al.*, 2011; Numanoi, 1934; Steel, 1993; Ziegler, 1997; Ziegler *et al.*, 2007). Since ACC is about 10 times more soluble than crystalline calcium carbonate phases (Brečević and Nielsen, 1989), high relative amounts of ACC within proximal layers make perfect sense, when large amounts of calcium carbonate need to be stored and recycled in order to quickly restore the protective function of a thick cuticle (Hild *et al.*, 2008).

4.2 Calcite orientation patterns in *A. vulgare* and *P. scaber* – comparison of results obtained by Raman and EBSD

Using two independent methods, SCμ-RSI and EBSD, we show for the first time that the calcite containing layer of the tergite cuticle of *A. vulgare* and *P. scaber* contain aggregates of similar crystallographic orientations. Figures 9 and 10 demonstrate the high correspondence of the results

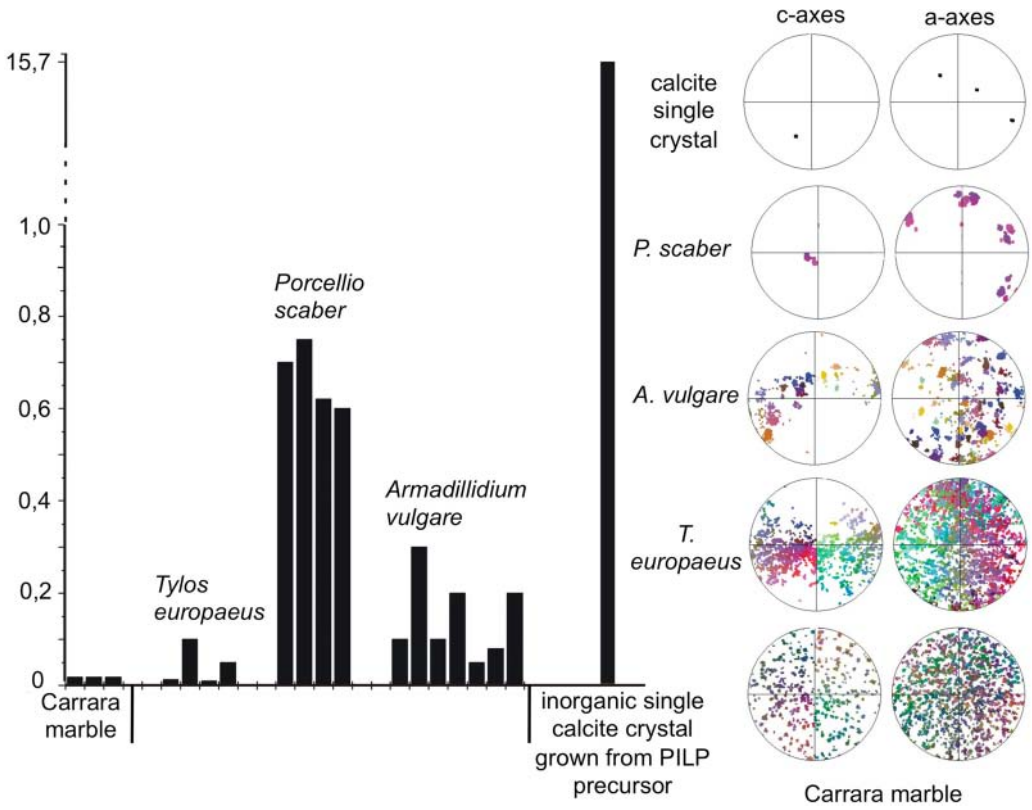

Fig. 11. Comparison of texture sharpness between the isopods *A. vulgare*, *P. scaber* and *T. europeus* relative to the texture sharpness present in two non-biologic carbonates: 1. Carrara marble, a recrystallized carbonate deposit and 2. Inorganic calcite crystals grown from a polymer induced liquid precursor phase (PILP) (Gong *et al.* 2010). The values for texture sharpness were normalized to the size of the individual EBSD maps and expressed as the multible of the random distribution value of 1. Well visible is the difference in texture sharpness between the three isopod species *T. europaeus, P. scaber* and *A. vulgare,* as well as the comparatively high texture in *P. scaber* and the surprisingly low ordered arrangement of calcite crystals in *T. europaeus*. On the right-hand side of the Figure representative EBSD data sets are presented in pole figures of: 1. Calcite single crystal, 2. The ordered arrangement of calcite in *P. scaber*, 3. The significantly less ordered arrangement of calcite in *A. vulgare*, 4. The weak texture in *T. europaeus* and 5. The almost unoriented calcite crystal agglomeration in the recrystallized marble.

gained from Raman and EBSD measurements regarding the size and the shape of these domains. Exact quantitative data on calcite crystal orientation cannot be achieved by SCμ-RSI and the subsequent comparison of CR values at different (0°and 90°) polarization of the incident laser light. However, the method allows estimating more general data on crystallographic orientation when changes in CR values of sets of aggregates are considered (Figs. 9C, D and 10C, D). In *A. vulgare* the individual CR values change between factors of about 1 and more than 2 for the sagittal plane (Fig. 9C), and between 1 and almost 3 for the tangential plane (Fig. 9D). The high variations in the CR changes for both, sagittal and tangential planes suggest a preference in the orientation of calcite *c*-axis of the aggregates parallel to the surface of the cuticle and some variation in the $x-y$ direction. This is confirmed by calcite-axes orientation variations deduced from EBSD (Fig. 9E). In *P. scaber* the CR values for calcite change by factors of about 1.3 and 2 for the sagittal plane (Fig. 10C) and by 1.6 and 2.6 for the tangential plane (Fig. 10D). Although for *P. scaber* the number of regions analyzed by Raman microscopy is too low to obtain representative data, the lower range of CR changes in comparison to that of *A. vulgare* (Fig. 9) is also in accordance to the results obtained by EBSD that suggest, that in contrast to the cuticle of *A. vulgare,* calcite crystals are grouped into few zones with similar orientations. Altogether it appears that polarized SCμ-RSI is a powerful tool to distinguish calcite domains of different crystallographic orientation with the advantage over EBSD that amorphous carbonate phases can be distinguished as well. The disadvantage, however, is that estimates in orientation of individual domains remains ambiguous since the change in CR depends on the initial orientation of calcite towards the direction of the polarisation of the incident light. Furthermore, the lack of significant changes in CR whenever calcite crystallites are mixed with regions containing ACC also seems to limit the application of this method. Here it is important to note that in our measurements on geological calcite the angle between the calcite and the direction (z) of the incident light remained constant. Decreasing this angle towards 0° will result in larger changes of CR between 2.5 and 3 for 0° and 90° polarization and to higher absolute CR values, whereas increasing the angle towards 90° will have the opposite effect. Therefore, future experiments on *c*-axis variations will teach us how absolute values of CR can contribute calcite crystal orientation analysis by polarized SCμ-RSI.

4.3 Calcite crystal orientation patterns deduced from EBSD measurements

Our EBSD analysis revealed that calcite in the tergite cuticle of the two species is organized in at least 4 hierarchical levels. The first level is given by 20 to 30 nm sized,

calcite nanoparticles that form the mineral phase of the exocuticle in *A. vulgare* and *P. scaber* at the nanoscale (Hild *et al.*, 2008). The EBSD maps indicate that these crystallized nanoparticles assemble to a few hundred nm sized mesocrystalline clusters. The mesocrystalline structure of the clusters can be well observed as small variations in the colour within the individual patches of the EBSD maps (Figs. 9E and 10E) and represent the second hierarchical level. On the third level these clusters assemble again and form fairly co-oriented second-order mesocrystalline aggregates.

The degree of crystallographic orientational coherence is high for the first three levels of hierarchy and is comparable for *A. vulgare* and *P. scaber.* This changes on the next hierarchical level, where strong crystallographic coherence is lacking in both species. Thus, we observe a short- and long-range crystallographic order of calcite that is distinct on the different scale levels. The short-range order (on the nano- and even microscale) of calcite is high while the long-range order (above 50–100 micrometer) of calcite is low for the two investigated isopods.

Interestingly, the high short-range order is similar, and the low long-range crystallographic coherence is different for the two isopod species and can be expressed as the texture sharpness. The distribution of crystallographic axes orientations is displayed by shading densities. These are generally normalized to the value of 1 for the average. As the random distribution of discrete orientations corresponds to a uniform distribution, densities in a textured sample are expressed as the of a uniform average density or random distribution (Kocks *et al.* 1998). The texture sharpness value of an EBSD map is defined as multiple of a random distribution. This value is normalized to the size of each individual map. For *A. vulgare* texture sharpness of aggregates (Fig. 11) is higher than for the beach dwelling supralittoral isopod *Tylos europaeus* (manuscript in preparation) but is still considerably lower than for *P. scaber.* When taking into account differences in the surface topology between *A. vulgare* and *P. scaber*, *e.g.* the presence of cuticular tubercles in *P. scaper* that are lacking in *A. vulgare,* the texture sharpness in *P. scaber* is underestimated since most planes cut through regions in which the cuticle of the tubercle is oblique to the polished plane analysed. Thus, in *P. scaber* orientation of the calcite *c*-axis is much better aligned parallel to the local cuticle surface in comparison to that in *A. vulgare*. In *A. vulgare* some horizontal alignment is still present and the texture sharpness is higher than in *T. europaeus,* in which texture sharpness is almost as low as in recrystallized non-biologic calcite, *e.g.* a marble (Fig. 11).

4.4 Texture-Function relation in cuticle of *A. vulgare* and *P. scaber*

Biological hard tissues are used for protection and functionality. This requires that the material is stiff and tough but not brittle (*e.g.* Currey, 1999; Meyers *et al.*, 2008; Dunlop and Fratzl, 2010). These properties are achieved through hierarchy, incorporation of mineral into an organic matrix, and specific orientation patterns of both, the organic and inorganic components (*e.g.* Weiner and Addadi, 1997; Fratzl *et al.*, 2007; Wang and Gupta, 2011). Texture-function relationships are best studied in bone (*e.g.* Weiner and Wagner, 1998, Currey, 1999; Weinkammer and Fratzl, 2011), and mollusc and gastropod nacre (*e.g.* Chateigner *et al.*, 2000; Barthelat and Espinoza, 2007; Ouhenia *et al.*, 2008; Barthelat, 2010; Wang and Gupta, 2011; Cartwright and Checa, 2012). Selective studies on other biological hard tissues have also been performed such as on human and sea urchin teeth (Zaslansky *et al.*, 2006; Wang *et al.*, 1995), sea urchin spines (*e.g.* Seto, *et al.* 2012), shells of molluscs, brachiopods and oysters (Schmahl *et al.*, 2008; Merkel *et al.*, 2009; Checa *et al.*, 2009; Frida *et al.*, 2010; Schmahl *et al.*, 2012), eggshells (Dunn *et al.*, 2011), corals (Vielzeuf *et al.*, 2010) and insect and crustacean cuticles (Vincent and Wegst, 2004; Raabe *et al.*, 2006; Raue *et al.*, 2008; Al-Sawalmih *et al.*, 2008). All these studies demonstrate clearly the biological control on mineral orientation and the ability of organisms to adjust crystal orientation to specific functional and ecological requirements. The comparison between calcite texture in isopod cuticle and that in other carbonate-based skeletons and teeth (Chateigner *et al.* 2000; Dahlbeck *et al.*, 2006; Griesshaber *et al.*, 2012; Goetz *et al.*, 2010, 2011; Hahn *et al.*, 2012; Schmahl *et al.*, 2012) shows that the overall preferred orientation of calcite is strikingly low in the tergites of the investigated isopods. In addition, in shells and teeth calcite *c*-axis orientation is perpendicular to the outer surface of the structure and rotates with its curvature (*e.g.* Schmahl *et al.*, 2004; Dahlbeck *et al.*, 2006; Ouhenia *et al.*, 2008; Griesshaber 2012).

Within the Crustacea there seems to be higher variation in *c*-axis orientation. In the carapace of the lobster *Homarus americanus,* a large crustacean belonging to the order of Decapoda, that has a similar distribution of calcite and ACC as in isopods (Al-Sawalmih *et al.*, 2008), texture analysis of calcite revealed a high texture sharpness with the *c*-axis oriented perpendicular to the cuticle surface as in molluscs and brachiopods. However, in the shell of the giant barnacle *Austromegabalanus psittacus,* a large sessile crustacean belonging to the taxon of Cirripedia, the orientation of the calcite crystallographic *c*-axis shifts between several layered compartments of the shell. It is randomly oriented in the outer and perpendicular to the surface in the subjacent shell layer (Rodriguez-Navarro *et al.*, 2006).

At present, it is difficult to unambiguously assess the texture-function relation for isopod tergite cuticle. However, hints may arise from the comparative approach we presented here. As already mentioned in the Introduction, conglobating species like *A. vulgare and Tylos europaeus* (Griesshaber *et al.*, manuscript in preparation) rely on the mechanical strength of the tergite cuticle to avoid predation, whereas *P. scaber* clings tightly to the substrate and can run away as a second option. Thus, the ability to withstand mechanical loads has to be high in the conglobating species in comparison to *P. scaber* that requires a more flexible and lightweight cuticle. In conglobating species, forces the cuticle has to withstand during predation likely have no sharp directional preference. For instance when the isopod does not control its position when rolled up, and a predator has no preference from which direction it applies force to the sphere. Therefore, the high degree of isotropy in the cuticle may be an adaptation to predation.

In the same way more directional forces during predation, for instance when a predator tries to lift of the animal from the substrate to access the softer ventral cuticle, may explain the higher texture sharpness in the tergite cuticle of *P. scaber*. It appears possible, that the preference of the calcite *c*-axis orientation parallel to the bilateral symmetry plane of the animal, may arise from internal forces applied by longitudinally oriented muscles of the isopod in order to prevent exposure of the flexible cuticular membranes between the tergites that are not reinforced by mineral. Possibly, the preference for calcite *c*-axis orientation parallel to the cuticle surface as observed in *A. vulgare* and *P. scaber* is an adaptation to internal forces the cuticle has to withstand after the moulting. In general the animals grows after each moult. Therefore, the new cuticle that is larger than the old one has to be stretched by uptake of water into the hemolymph space. This puts tensile stress on the organic matrix that is oriented parallel to the cuticle surface, even within the cuticular tubercles present in the tergites of *P. scaber*. In order to maintain body shape the cuticle becomes mineralised in this stressed state. It thus may be that the exocuticle, that is mineralised before the endocuticle, has to take up multidirectional in-plane mechanical load from the organic matrix when the hydrostatic pressure within the animals is relaxed.

5. Conclusions

In a combined analytical approach using polarized SCμ-RSI and EBSD we investigated calcite crystal orientation and distribution in the cuticle of the two terrestrial isopods *A. vulgare* and *P. scaber*. This is the first study where calcite crystal orientation in a biological material is deduced from polarized SCμ-RSI experiments. Furthermore, it is the first EBSD analysis performed on isopod cuticle and we show first EBSD results that are obtained on microtome polished carbonate biological hard tissues.

In the investigated isopod species calcite crystal orientation has a mesocrystalline arrangement with calcite being organized on several hierarchical scale levels. Calcite orientation pattern and sharpness in *A. vulgare* and *P. scaber* is extremely distinct to that observed in other carbonate-based biological materials. In teeth or shells of other animals texture sharpness is high at all scale levels and is also high over large portions of the hard tissue. This is not the case in the investigated isopod cuticle. On the nanometer scale and up to 50–100 micrometer we see in both isopod species a high preferred orientation of calcite that decreases significantly on larger scales. In *A. vulgare* clusters of calcite nanocrystalls are assembled into numerous randomly oriented aggregates, while in *P. scaber* calcite crystal conglomeration is more coherent. In addition, even though *A. vulgare* and *P. scaber* belong to the same isopod suborder (Oniscidea) and live in similar habitats the two isopods have a distinct calcite crystal orientation pattern on the scale of several tenth of micrometers. The almost random orientation of calcite in *A. vulgare* results in an isotropic distribution of material properties (*e.g.* mechanical properties) within the cuticle, while the more oriented pattern of calcite in running *P. scaber* effects a more anisotropic distribution of material properties in the cuticula. We attribute these differences to predation avoidance requirements. This is one of the very few studies where mineral texture patterns are investigated in relation to specific behavioral requirements.

Acknowledgements. We thank K. Huemer for polarized SCμ-RSI measurements on geological calcite. This work was supported by the DFG within the priority program SPP1420 (Zi 368/ 8–2).

References

[1] Al-Sawalmih, C. Li, S. Siegel, H. Fabritius, D. Raabe, P. Fratzl, O. Paris, *Adv. Fuct. Mat.* **2008**, *18*, 3307.
[2] F. Barthelat, H. D. Espinosa, *Exp. Mech.* **2007**, *47*, 311.
[3] F. Barthelat, *Bioinsp. Biomim.* **2010**, *5*, 1.
[4] A. Becker, A. Ziegler, M. Epple, *Dalton Transactions* **2005**, *10*, 1814.
[5] F. Boßelmann, P. Romano, H. Fabritius, D. Raabe, M. Epple, *Thermochim. Acta* **2007**, *463*, 65.
[6] Y. Bouligand, *Tissue and Cell* **1972**, *4*, 189.
[7] L. Brečević, A. E. Nielsen, *J. Crystal Growth* **1989**, *98*, 504.
[8] J. Cartwright, A. G. Checa, *J. R. Soc. Interface* **2007**, *4*, 491.
[9] D. Chateigner, C. Hedegaard, H.-R. Wenk, *J. Struct. Geol.* **2000**, *22*, 1723.
[10] A. G. Checa, F. J. Esteban-Delgado, J. Ramirez-Rico, A. B. Rodriguez-Navarro, *J. Struct. Biol.* **2009**, *167*, 261.
[11] J. D. Currey, *J. Exp. Biol.* **1999**, *202*, 3285.
[12] J. W. C. Dunlop, P. Fratzl, *Annu. Rev. Mater. Res.* **2010**, *10*, 1.
[13] P. Dahlbeck, J. England, M. Cussack, M. Lee, A. E. Fallick, *Eur. J. Mineral.* **2006**, *18*, 601.
[14] I. C. Dunn, A. B. Rodriguez-Navarro, K. Mcdade, M. Schmutz, R. Preisinger, D. Waddington, P. W. Wilson, M. M. Bain, *Animal Genetics* **2011**, DOI: 10.1111/j.1365–2052.2011.02280.
[15] H.-O. Fabritius, E. S. Karsten, K. Balasundaram, S. Hild, K. Huemer, D. Raabe, *Z. Kristallogr.* **2012**, DOI: 10.1524/zkri.2012.1532.
[16] P. Fratzl, H. S. Gupta, F. D. Fischer, O. Kolednik, *Adv. Mater.* **2007**, *19*, 2657.
[17] J. Frida, M. Klicnarova, B. Frydova, M. Mergl, *Bull. Geosci,* **2010**, *85*, 645.
[18] A. Goetz, E. Griesshaber, W. W. Schmahl, *Solid State Phenomena*, **2010**, *160*, 229.
[19] A. Goetz, D. R. Steinmetz, E. Griesshaber, S. Zaefferer, D. Raabe, K. Kelm, S. Irsen, A. Sehrbrock, W. W. Schmahl, *Acta Biomater.* **2011**, *7*, 2237.
[20] E. Griesshaber, W. W. Schmahl, R. Neuser, Th. Pettke, M. Blüm, J. Mutterlose, U. Brand, *Amer. Min.* **2007**, *92*, 722.
[21] E. Griesshaber, A. Goetz, L. Howard, A. Ball, S. Ruff, W. W. Schmahl, *BBN* **2012**, *1*, 133.
[22] H. Gong, M. Pluntke, O. Marti, P. Walther, L. Gower, H. Cölfen, D. Volkmer, *Colloid Surf.* **2010**, *354,* 279.
[23] S. Hahn, R. Rodolfo-Metalpa, E. Griesshaber, W. W. Schmahl, D. Buhl, J. M. Hall-Spencer, C. Baggini, K. T. Fehr, A. Immenhauser, *Biogeosciences Discuss.* **2012**, *9*, 1897.
[24] S. Hild, O. Marti, A. Ziegler, *J. Struct. Biol.* **2008**, *163*, 100.
[25] S. Hild, F. Neues, N. Žnidaršič, J. Štrus, M. Epple, O. Marti, A. Ziegler, *J. Struct. Biol.* **2009**, *168*, 426.
[26] U. F. Kocks, C. N. Tome, H.-R. Wenk, Texture and Anisotropy, Cambridge University Press, Cambridge U.K. 1998, 238 pp.
[27] I. I. Kondilenko, P. A. Korotkov, V. A. Klimenko, *Optics and Spectroscopy* **1976**, *40*, 402.
[28] M. A. Meyers, P.-Y. Chen, A. Y.-M. Lin, Y. Seki, *Prog. Mat. Sci.* **2008**, *53*, 1.
[29] C. Merkel, J. Deuschle, E. Griesshaber, S. Enders, E. Steinhauser, R. Hochleitner, U. Brand, W. W. Schmahl, *J. Struct. Biol.* **2009**, *168*, 396.
[30] F. Neues, A. Ziegler, M. Epple, *Cryst. Eng. Comm.* **2007**, *9*, 1245.
[31] F. Neues, S. Hild, M. Epple, O. Marti, A Ziegler, *J. Struct. Biol.* **2011**, *175*, 10.

[32] S. Nikolov, M. Petrov, L. Lyperakis, M. Friák, C. Sachs, H. Fabritius, D. Raabe, J. Neugebauer, *Adv. Mat.* **2010**, *22*, 519.
[33] S. Nikolov, H. Fabritius, M. Petrov, M. Friák, L. Lymperakis, C. Sachs, D. Raabe, J. Neugebauer, *J. Mech. Behav. Biomed. Mat.* **2011**, *4*, 129.
[34] H. Numanoi, *J. Fac. Sci. Tokyo Univ.* **1934**, *4*, *3*, 351.
[35] S. Ouhenia, D. Chateigner, M. A. Belkhir, E. Guilmeau, *J. Struct. Biol.* **2008**, *163*, 175.
[36] S. P. S. Porto, J. A. Giordmaine, T. C. Damen, *Phys. Rev.* **1966**, *147*, 608.
[37] D. Raabe, P. Romano, C. Sachs, H. Fabritius, A. Al-Sawalmih, S.-B. Yi, G. Servos, H. G. Hartwig, *Mat. Sci. Eng. A* **2006**, *421*, 143.
[38] L. Raue, H. Klein, D. Raabe, H. Fabritius, Proc. 15th International Conference on the Texture of Materials (ICOTOM 15), Pennsylvania, USA, 2008.
[39] A. B. Rodriguez-Navarro, C. Cabralde-Melo, N. Batista, N. Morimoto, P. Alvarez-Lloret, M. Ortega-Huertas, V. M. Fuenzalida, J. I. Arias, J. P. Wiff, J. L. Arias, *J. Struct. Biol.* **2006**, *156*, 355.
[40] B. Seidl, K. Huemer, F. Neues, S. Hild, M. Epple, A. Ziegler, *J. Struct. Biol.* **2011**, *174*, 512.
[41] B. Seidl, A. Ziegler, ZooKeys, 2011, DOI: 10.3897/zookeys.2011.2294.
[42] J. Seto, Y. Ma, S. Davis, F. Meldrum, A. Gourrier, Y.-Y. Kim, U. Schilde, M. Sztucki, M. Burghammer, S. Maltsev, C. Jäger, H. Cölfen, *PNAS* **2012**, *109*, 3699.
[43] W. W. Schmahl, E. Griesshaber, R. Neuser, A. Lenze, R. Job, U. Brand, *Eur. J. Mineral.* **2004**, *16*, 693.
[44] W. W. Schmahl, E. Griesshaber, C. Merkel, K. Kelm, J. Deuschle, R. D. Neuser, A. J. Götz, A. Sehrbrock, W. Mader, *Min. Mag.* **2008**, *72*, 541.
[45] W. W. Schmahl, E. Griesshaber, K. Kelm, A. Goetz, G. Jordan, A. Ball, D. Xu, C. Merkel, U. Brand, *Z. Krist. Cryst. Mat.* 2012, doi: 10.1524/zkri.2012.1479.
[46] H. Schmalfuss, *Symp. Zool. Soc. London* **1984**, *53*, 49.
[47] N. H. Schmidt, N. O. Olesen, N. O. *Canad. Mineral.* **1989**, *27*, 15.
[48] G. Turrell, J. Raman Spectr. **1984**, *15*, 103.
[49] C. G. H. Steel, *Canad. J. Zool.* **1993**, *71*, 4.
[50] D. Vielzeuf, N. Floquet, D. Chatain, F. Bonnete, D. Ferry, J. Garrabou, E. Stolper, *Amer. Mineral.* **2010**, *95*, 242.
[51] J. F. V. Vincent, U. G. K. Wegst, *Arthopod Struct. Dev.* **2004**, *33*, 187.
[52] R. Z. Wang, L. Addadi, S. Weiner, *Phil. Trans. R. Soc. London B* **1995**, *352*, 469.
[53] R. Z. Wang, H. S. Gupta, Annu. *Rev. Mater. Res.* **2011**, *41*, 41.
[54] J. Wang, Q. Cheng, Z. Tang, *Chem. Soc. Rev.* **2012**, *41*, 1111.
[55] S. Weiner, L. Addadi, *J. Mater. Chem.* **1997**, *7*, 689.
[56] S. Weiner, H. D. Wagner, *Annu. Rev. Mater. Sci.,* **1998**, *28*, 271.
[57] R. Weinkamer, P. Fratzl, *Mat. Sci. Eng. C* **2011**, *31*, 1164.
[58] P. Zaslansky, R. Shahar, A. A. Friesem, S. Weiner, *Adv. Funct. Mat.* **2006**, *16*, 1925.
[59] A. Ziegler, *J. Struct. Biol.* **1994**, *112*, 110.
[60] A. Ziegler, *Tissue and Cell,* **1997**, *29*, 63.
[61] A. Ziegler, M. Hagedorn, G. A. Ahearn, T. H. Carefood, *J. Comp. Physiol. B* **2007**, *177*, 99.